



NATURAL CONVECTION IN ENCLOSURE WITH DISCRETE ISOTHERMAL HEATING FROM BELOW

Goutam Saha¹, Sumon Saha^{2*}, M. Quamrul Islam² and M. A. Razzaq Akhanda³

¹Department of Arts and Sciences, Ahsanullah University of Science and Technology (AUST), Dhaka-1215, Bangladesh. ²Department of Mechanical Engineering, Bangladesh University of Engineering and Technology (BUET), Dhaka-1000, Bangladesh. ³Department of Mechanical and Chemical Engineering, Islamic University of Technology (IUT), Board Bazar, Gazipur-1704, Bangladesh. Email: *sumonsaha@me.buet.ac.bd

Abstract

Natural convection in two-dimensional rectangular enclosure is studied numerically using a finite element method. In the present study, top wall is considered adiabatic, two vertical walls are maintained at constant low temperature, the bottom wall is maintained at constant high temperature and the non-heated parts of the bottom wall are considered adiabatic. The aim of this work is to demonstrate the capabilities of this numerical methodology for handling such problems. The pressure-velocity form of the Navier–Stokes equations and energy equation are used to represent the mass, momentum, and energy conservations of the fluid medium in the enclosure. The finite element formulations of the dimensionless governing equations with the associated boundary conditions are solved by a nonlinear coupled solution algorithm using six-noded triangular element discretization scheme for all the field variables. The Grashof number is varied from 10^3 to 10^6 and Prandtl number is taken as 0.71. This study has reported the effect of various aspect ratios, ranging from 0.5 to 1, and inclination angles of the enclosure from 0° to 30° on the thermo-fluid characteristics. Results are presented in the form of streamline and isotherm plots as well as the variation of the Nusselt number at the heat source surface under different conditions.

Keywords: Natural convection, rectangular enclosure, aspect ratio, finite element method, Nusselt number.

NOMENCLATURE

A	Aspect ratio of the enclosure	Greek Symbols	
g	Gravitational acceleration	α	Thermal diffusivity
Gr	Grashof number	β	Thermal expansion coefficient
H	Height of the enclosure	θ	Dimensionless temperature
k	Thermal conductivity of air	ν	Kinematic viscosity
L	Length of the heat source	ρ	Fluid density
p	Pressure	Φ	Inclination angle
P	Dimensionless pressure	ε	Heat source length
Pr	Prandtl number	ΔT	Temperature difference
T	Temperature	Subscript	
u, v	Velocity component in x and y direction	c	Cold wall
U, V	Dimensionless velocity component in x and y direction	h	Hot wall
W	Width of the enclosure		
x, y	Cartesian coordinates		
X, Y	Dimensionless cartesian coordinates		

1. Introduction

Effective cooling of electronic components has become increasingly important as power dissipation and component density continue to increase substantially with the fast growth of electronic technology. It is very important that such cooling systems are designed in the most efficient way and the power requirement for the cooling is minimized. The electronic components are treated as heat sources embedded on flat surface (Incropera, 1988 and Jaluria, 1985). In many applications natural convection is the only feasible mode of cooling of the heat source. Besides cooling of the electronic components, there are numerous other practical applications of natural convective cooling in rectangular enclosures with various combinations of the temperature gradients, cavity aspect ratios, placement of the heat source and cold surfaces, etc.

Following the pioneering numerical work of Chu *et al.* (1976) on two-dimensional, laminar natural convection cooling of a single, isothermal flush-mounted heater on a vertical wall inside an air-filled rectangular enclosure, the heat transfer problem of natural convection in a discretely heated enclosure is of great research interest as indicated by the considerable research activities on this subject. A natural convection heat transfer experiment in a tall vertical rectangular enclosure (aspect ratio 16.5) with an array of eleven discrete flush-heaters has been performed by Keyhani *et al.* (1988). It was found that the discrete heating in the enclosure results in a significantly augmented local heat transfer rate over that for an enclosure with the uniformly heated vertical wall. A follow-up study (Keyhani *et al.*, 1988) for a vertical enclosure aspect ratio 4.5 with three flush heaters further revealed that the temperature of the heaters is strongly affected by the stratification of fluid inside the enclosure. Moreover, the effects of enclosure width and Prandtl number on natural convection liquid cooling of discrete flush heaters in a tall enclosure cooled from the top has been investigated experimentally and numerically (Carmona and Keyhani, 1989 and Prasad *et al.*, 1990). Refai Ahmed and Yovanovich (1991) performed a numerical study to examine the influence of discrete heat source location on natural convection heat transfer in a vertical square enclosure. Furthermore, the temperature field of natural convection within a discretely heated vertical enclosure with single and dual heaters configuration has been visualized using Mach-Zehnder interferometry (Chadwick *et al.*, 1991).

The problem of convective heat transfer in an enclosure has been studied extensively because of the wide application of such process. Ostrach (1988) provided a comprehensive review article and extensive bibliography on natural convection in cavities. Other articles on the topic published are Valencia and Frederick (1989), Selamet *et al.* (1992), Hasnaoui *et al.* (1992), Papanicolaou and Gopalakrishna (1995), Sundstrom and Kimura (1996), Hsu and Chen (1996), Elsherbiny *et al.* (1982), and Nguyen and Prudhomme (2001), among others, who investigated natural convection in rectangular enclosures under various configurations and orientations. Anderson and Lauiat (1986) studied the natural convection in a vertical square cavity heated from bottom and cooled from one side. Convection in a similar configuration where the bottom wall of the rectangular cavity was partially heated with cooling from one side was studied by November and Nansteel (1986). It was reported that the heated fluid layer near the bottom wall remains attached up to the turning corner. Ganzarolli and Milanez (1995) performed numerical study of steady natural convection in rectangular enclosures heated from below and symmetrically cooled from the sides. The size of the cavity was varied from square to shallow where the cavity width was varied from 1-10 times of the height. The heat source, which spanned the entire bottom wall, was either isothermal or at constant heat flux condition. Aydin and Yang (2000) numerically investigated the natural convection of air in a vertical square cavity with localized isothermal heating from below and symmetrical cooling from sidewalls. The top wall as well as non-heated parts of the bottom wall was considered adiabatic. The length of the symmetrically placed isothermal heat source at the bottom was varied. Two counter rotating vortices were formed in the flow domain due to natural convection. The average Nusselt number at the heated part of the bottom wall was shown to increase with increasing Rayleigh number as well as with increasing length of the heat source.

The geometry and coordinate system of the problem under consideration is depicted in Fig. 1. It consists of a rectangular enclosure of dimension, $W \times H$, whose sidewalls are kept at a constant low temperature, T_c . The aspect ratio of the enclosure is defined as $A = H/W$. The bottom wall is maintained

at constant high temperature, T_h and length L . The remaining parts of the bottom wall and the entire upper wall are adiabatic. The present study reports the computations for enclosures at various aspect ratios, ranging from 0.5 to 1, and inclination angles from 0° to 30° . The natural convection parameter, Grashof number, Gr is varied from 10^3 to 10^6 . Also the ratio of the heating element to the enclosure width, $\varepsilon = L/W$ and is varied from 0.2 to 0.8.

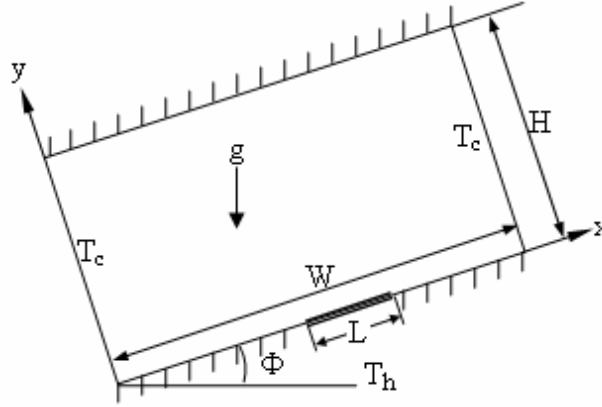


Fig. 1: Schematic diagram of the physical system.

2. Mathematical Model

Natural convection is governed by the differential equations expressing conservation of mass, momentum and energy. The present flow is considered steady, laminar, incompressible and two-dimensional. The viscous dissipation term in the energy equation is neglected. The Boussinesq approximation is invoked for the fluid properties to relate density changes to temperature changes, and to couple in this way the temperature field to the flow field. Then the governing equations for steady natural convection can be expressed in the dimensionless form as:

$$U \frac{\partial U}{\partial X} + V \frac{\partial U}{\partial Y} = 0 \quad (1)$$

$$U \frac{\partial U}{\partial X} + V \frac{\partial U}{\partial Y} = -\frac{\partial P}{\partial X} + \left(\frac{\partial^2 U}{\partial X^2} + \frac{\partial^2 U}{\partial Y^2} \right) + (Gr \sin \Phi) \theta \quad (2)$$

$$U \frac{\partial V}{\partial X} + V \frac{\partial V}{\partial Y} = -\frac{\partial P}{\partial Y} + \left(\frac{\partial^2 V}{\partial X^2} + \frac{\partial^2 V}{\partial Y^2} \right) + (Gr \cos \Phi) \theta \quad (3)$$

$$U \frac{\partial \theta}{\partial X} + V \frac{\partial \theta}{\partial Y} = \frac{1}{Pr} \left(\frac{\partial^2 \theta}{\partial X^2} + \frac{\partial^2 \theta}{\partial Y^2} \right) \quad (4)$$

where X and Y are the coordinates varying along horizontal and vertical directions, respectively, U and V are the velocity components in the X and Y directions, respectively, θ is the temperature, P is the pressure, and Φ is the inclination angle of the enclosure with the horizontal direction, Gr and Pr , are the Grashof number and Prandtl number, respectively, and they defined as

$$Gr = \frac{g \beta \Delta T W^3}{\nu^2} \quad \text{and} \quad Pr = \frac{\nu}{\alpha} \quad (5)$$

The dimensionless parameters in the equations above are defined as follow:

$$X = \frac{x}{W}, \quad Y = \frac{y}{W}, \quad U = \frac{uW}{\nu}, \quad V = \frac{vW}{\nu}, \quad P = \frac{pW^2}{\rho \nu^2}, \quad \theta = \frac{T - T_c}{\Delta T}, \quad \Delta T = T_h - T_c \quad (6)$$

where ρ , β , ν , α and g are the fluid density, coefficient of volumetric expansion, kinematic viscosity, thermal diffusivity, and gravitational acceleration, respectively.

The boundary conditions for the present problem are specified as follows:

Top wall:

$$U = V = 0, \frac{\partial \theta}{\partial Y} = 0$$

Right and left wall:

$$U = V = 0, \theta = 0$$

Bottom wall:

$$U = V = 0$$

(7)

$$\frac{\partial \theta}{\partial Y} = 0 \quad \text{for} \quad 0 < X < 0.5 - \frac{\varepsilon}{2} \quad \text{and} \quad 0.5 + \frac{\varepsilon}{2} < X < 1$$

$$\theta = 1 \quad \text{for} \quad 0.5 - \frac{\varepsilon}{2} \leq X \leq 0.5 + \frac{\varepsilon}{2}$$

The average Nusselt number (Luo and Yang, 2007) can be written as

$$Nu = -\frac{1}{\varepsilon} \int_0^\varepsilon \frac{\partial \theta}{\partial Y} dX$$

(8)

3. Finite Element Formulation

The basic idea of the solution algorithm proposed in this paper is to use the two momentum equations for solving both of the velocity components, use the continuity equation for solving the pressure, and use the energy equation for solving the temperature. The element assumes linear interpolation for the velocity components, the pressure, and the temperature as

$$U(X, Y) = N_i U_i$$

(9a)

$$V(X, Y) = N_i V_i$$

(9b)

$$P(X, Y) = N_i P_i$$

(9c)

$$\theta(X, Y) = N_i \theta_i$$

(9d)

where $i = 1, 2, 3, 4, 5, 6$; and N_i is the element interpolation functions.

The two momentum equations, Eqs. (2), (3), are discretized using the conventional Bubnov-Galerkin's method. However, a special treatment of the convection terms is incorporated. Using the standard Galerkin approach, each momentum equation is multiplied by weighting functions, N_i , and then the diffusion terms are integrated by parts using the Gauss theorem to yield the finite element equations in the form

$$AU = R_{PX} + R_U + R_a$$

(10a)

$$AV = R_{PY} + R_V + R_b$$

(10b)

where the coefficient matrix A contains the known contributions from the convection term. The load vectors on the right-hand side of Eqs. (10a), (10b) are defined by

$$R_{PX} = -\int_{\Omega} N_i \frac{\partial P}{\partial X} d\Omega$$

(11a)

$$R_{PY} = -\int_{\Omega} N_i \frac{\partial P}{\partial Y} d\Omega$$

(11b)

$$R_U = \int_{\Gamma} N_i \left(\frac{\partial U}{\partial X} n_x + \frac{\partial U}{\partial Y} n_y \right) d\Gamma$$

(11c)

$$R_V = \int_{\Gamma} N_i \left(\frac{\partial V}{\partial X} n_x + \frac{\partial V}{\partial Y} n_y \right) d\Gamma$$

(11d)

$$R_a = \int_{\Omega} N_i (Gr \sin \theta) d\Omega \quad (11e)$$

$$R_b = \int_{\Omega} N_i (Gr \cos \theta) d\Omega \quad (11f)$$

where Ω is the element area and Γ is the element boundary.

To derive discretized pressure equation, the method of weighted residuals is applied to the continuity equation, Eq. (1),

$$\int_{\Omega} N_i \left(\frac{\partial U}{\partial X} + \frac{\partial V}{\partial Y} \right) d\Omega = - \int_{\Omega} \left(\frac{\partial N_i}{\partial X} U + \frac{\partial N_i}{\partial Y} V \right) d\Omega + \int_{\Gamma} N_i (U n_x + V n_y) d\Gamma = 0 \quad (12)$$

where the integrations are performed over the element domain Ω and along the element boundary Γ ; n_x and n_y are the direction cosines of the unit normal to the element boundary with respect to X and Y directions, respectively. Now we consider

$$A_{ii} U_i = - \sum_{j \neq i} A_{ij} U_j + f_i^U - \int_{\Omega} N_i \frac{\partial P}{\partial X} d\Omega \quad (13a)$$

$$A_{ii} V_i = - \sum_{j \neq i} A_{ij} V_j + f_i^V - \int_{\Omega} N_i \frac{\partial P}{\partial Y} d\Omega \quad (13b)$$

where f_i^U and f_i^V are the surface integral terms and the source term due to buoyancy. By assuming constant pressure gradient on an element, we get

$$U_i = \bar{U}_i - K_i^P \frac{\partial P}{\partial X} \quad (14a)$$

$$V_i = \bar{V}_i - K_i^P \frac{\partial P}{\partial Y} \quad (14b)$$

where

$$\bar{U}_i = \frac{1}{A_{ii}} \left(- \sum_{j \neq i} A_{ij} U_j + f_i^U \right) \quad (15a)$$

$$\bar{V}_i = \frac{1}{A_{ii}} \left(- \sum_{j \neq i} A_{ij} V_j + f_i^V \right) \quad (15b)$$

$$K_i^P = \frac{1}{A_{ii}} \left(\int_{\Omega} N_i d\Omega \right) \quad (15c)$$

By applying the element velocity interpolation functions, Eqs. (9a), (9b), into the continuity equation, Eq. (10), we have

$$\int_{\Omega} \frac{\partial N_i}{\partial X} (N_j U_j) d\Omega - \int_{\Omega} \frac{\partial N_i}{\partial Y} (N_j V_j) d\Omega + \int_{\Gamma} N_i (U n_x + V n_y) d\Gamma = 0 \quad (16a)$$

and introducing the nodal velocities U_j and V_j from Eqs. (14a), (14b), then Eq. (14) becomes,

$$\int_{\Omega} \frac{\partial N_i}{\partial X} (N_j K_j^P) \frac{\partial P}{\partial X} d\Omega + \int_{\Omega} \frac{\partial N_i}{\partial Y} (N_j K_j^P) \frac{\partial P}{\partial Y} d\Omega = \int_{\Omega} \frac{\partial N_i}{\partial X} (N_j \bar{U}_j) d\Omega + \int_{\Omega} \frac{\partial N_i}{\partial Y} (N_j \bar{V}_j) d\Omega - \int_{\Gamma} N_i (U n_x + V n_y) d\Gamma \quad (16b)$$

Finally, by applying the element pressure interpolation functions, Eq. (9c), the above element equations can be written in matrix form with unknowns of the nodal pressures as

$$(K_X + K_Y)P = F_U + F_V + F_C \quad (17)$$

where

$$K_X = \int_{\Omega} \frac{\partial N}{\partial X} (N_j K_j^P) \frac{\partial N}{\partial X} d\Omega \quad (18a)$$

$$K_Y = \int_{\Omega} \frac{\partial N}{\partial Y} (N_j K_j^p) \frac{\partial N}{\partial Y} d\Omega \quad (18b)$$

$$F_U = \int_{\Omega} N_j \bar{U}_j \frac{\partial N}{\partial X} d\Omega \quad (18c)$$

$$F_V = \int_{\Omega} N_j \bar{V}_j \frac{\partial N}{\partial Y} d\Omega \quad (18d)$$

$$F_C = - \int_{\Gamma} N (U n_x + V n_y) d\Gamma \quad (18e)$$

The above element pressure equations are assembled to form the global equations; boundary conditions for the specified nodal pressures are imposed prior to solving for the updated nodal pressures.

The finite element equations corresponding to the energy equation are derived using an approach similar to that used in deriving element momentum equations. The standard Galerkin method is applied to yield the element equations which can be written in matrix form as

$$K \theta = R \quad (19)$$

where

$$R = \frac{1}{Pr} \int_{\Gamma} N_i \left(\frac{\partial \theta}{\partial X} n_x + \frac{\partial \theta}{\partial Y} n_y \right) d\Gamma \quad (20)$$

These elements equations are again assembled to yield the global temperature equations. Appropriate boundary conditions are applied prior to solving for the new temperature values.

4. Numerical Procedure

The numerical procedure used to solve the governing equations for the present work is the combined finite element method. The application of this technique is well documented Zienkiewicz and Taylor (2000). It provides the smooth solutions at the interior domain including the corner regions. The non-linear parametric solution method is chosen to solve the governing algebraic equations. This approach will result in substantially fast convergence assurance. A non-uniform triangular mesh arrangement is implemented in the present investigation especially near the heated wall to capture the rapid changes in the dependent variables. Also six noded triangular elements are used in this paper since the six noded elements smoothly capture the non-linear variations of the field variables. All six nodes are associated with velocities as well as temperature, only the corner nodes are associated with pressure. Solutions were assumed to converge when the following convergence criteria was satisfied for every dependent variables at every point in the solution domain

$$\left| \frac{\Psi_{\text{new}} - \Psi_{\text{old}}}{\Psi_{\text{old}}} \right| \leq 10^{-6} \quad (21)$$

where Ψ represents a dependent variable U, V, P, and θ .

5. Results and Discussion

The working fluid is chosen as air with Prandtl number, $Pr = 0.71$. The normalized length of the constant heat source at the bottom wall, ϵ , is varied from 0.2 to 0.8. For each value of ϵ , the Grashof number, Gr , is varied from 10^3 to 10^6 , the aspect ratio, A , is varied from 0.5 to 1 while the inclination angle, Φ , is varied from 0° to 30° . To test and assess grid independence of the present solution scheme, many numerical runs are performed for higher Grashof number as shown in Table 1. These experiments reveal that a non-uniform spaced grid of 6394 elements for the solution domain is adequate to describe correctly the flow and heat transfer processes inside the enclosure. In order to validate the numerical model, the results are compared with those reported by Sharif and Mohammad (2005), for $A = 1.0$, $Gr = 10^3$ to 10^6 , $\epsilon = 0.2$ and $\Phi = 0^\circ$. In Table 2, a comparison of the average Nusselt number of the square enclosure is presented. The agreement is found to be excellent with a maximum discrepancy of about 1.01%, which validates the present computations indirectly.

Table 1: Comparison of the results for various grid dimensions ($A = 1.0$, $Gr = 10^6$, $\epsilon = 0.2$, $\Phi = 0^\circ$).

Elements	1970	2902	3540	4608	4828	6394	12606
Nu	16.229	16.854	16.379	16.487	16.534	16.581	16.581

Table 2: Comparison of the average Nusselt number of the square enclosure for $\epsilon = 0.2$ and $\Phi = 0^\circ$.

Gr	Average Nusselt Number, Nu		
	Sharif and Mohammad (2005)	Present Work	Error (%)
10^3	5.927	5.939	0.2
10^4	5.946	5.954	0.13
10^5	7.124	7.117	0.1
10^6	11.342	11.226	1.02

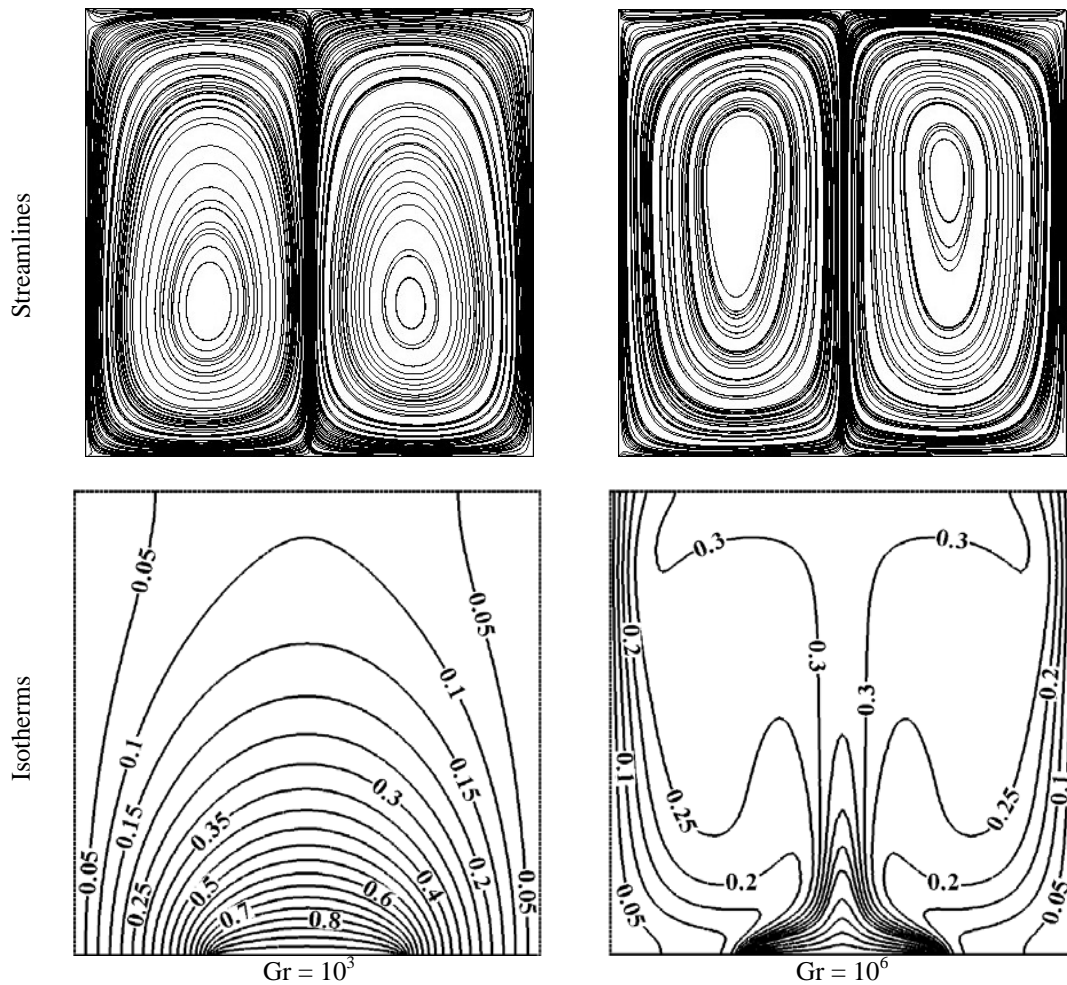


Fig. 2: Evolution of the flow in the enclosure with the variation of Gr for $A = 1.0$, $\epsilon = 0.4$ and $\Phi = 0^\circ$.

5.1 Effect of Grashof Numbers:

The evolution of the flow and thermal fields with Grashof number for an enclosure of aspect ratio, $A = 1$ for a representative case with $\epsilon = 0.4$ and $\Phi = 0^\circ$ is presented in Fig. 2. For various $Gr = 10^3$ - 10^6 , the flow pattern is characterized by two symmetrical rolls with clockwise and anti-clockwise rotations inside the enclosure. The hot fluid rises in the central region as a result of buoyancy forces, and then it descends downwards along the vertical walls and turns horizontally to the central region after hitting the bottom wall. The flow then rises along the vertical symmetry axis and gets blocked at the adiabatic

top wall, which turns the flow horizontally towards the cold vertical walls. Thus a pair of counter-rotating rolls is formed in the flow domain. At $Gr = 10^3$, as can be expected, heat transfer from the discrete heat source is essentially dissipated via a conduction-dominated mechanism as indicated by the isotherm pattern shown in Fig. 2. For $Gr > 10^3$, the buoyant convection flow in the central region between the rolls distorts the isotherms field. The distortion of the isotherm field increases with enhanced buoyancy as Gr increases, where the heat transfer becomes increasingly advection dominated. With increase of Gr to 10^6 a transformation from a primarily two symmetrical rolls pattern to a structure characterized by two large vortices near the central regions, moving towards upper wall. Therefore, the prevailing conductive heat transfer for $Gr = 10^3$ and the mushroom profile of the isotherms for $Gr = 10^6$ are presented in Fig. 2. Also viscous forces are more dominant than the buoyancy forces at lower Gr . At higher Gr when the intensity of convection increases significantly, the core of the circulating rolls moves up and the isotherm patterns changes significantly indicating that the convection is the dominating heat transfer mechanism in the enclosure.

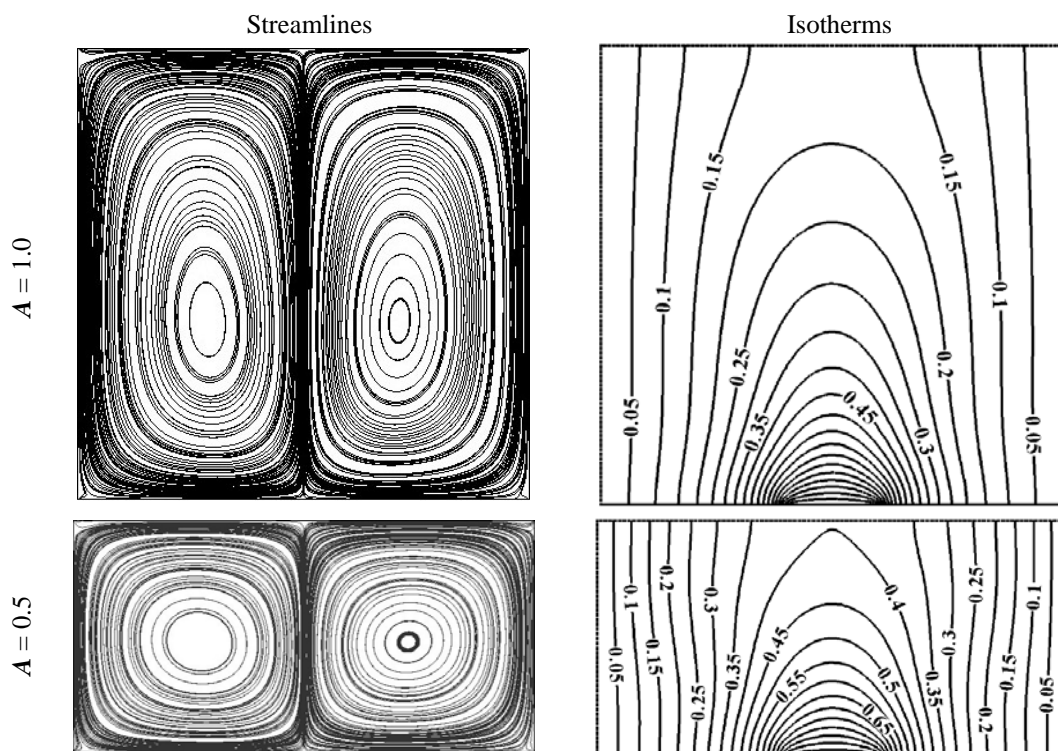


Fig. 3: Streamlines and isotherms profiles for different aspect ratios with $\varepsilon = 0.2$, $\Phi = 0^\circ$ and $Gr = 10^4$.

5.2 Effect of Aspect Ratio:

The buoyancy-driven flow and temperature fields inside the discretely heated enclosure of various aspect ratios are illustrated by means of contour maps of streamlines and isotherms, as exemplified in Figs. 3 for two different aspect ratios of 0.5 and 1.0 with $\Phi = 0^\circ$, $\varepsilon = 0.2$, and $Gr = 10^4$. As expected, due to the cold vertical walls, fluids rise up from middle portion of the bottom wall and flow down along the two vertical walls forming two symmetric rolls with clockwise and anti-clockwise rotations inside the cavity for all aspect ratios. However, in the convection region adjacent to the heat source, the isotherms become thinner and denser producing higher temperature gradients (increasing the overall Nusselt number) with increasing A , specially until the cavity changes from thin rectangle to square. This is due to the fact that the cavity volume increases with aspect ratio and more volume of cooling air is involved in cooling the heat source leading to better cooling effect.

For $A = 0.5$, the two convection rolls appeared in the rectangular cavity, each half filled up with clockwise or anti-clockwise circulation in a square area. At $Gr = 10^4$, the circulation intensity is not

much higher and the heat transfer is almost due to conduction, as evident from the isotherm plots (Fig. 3). During conduction dominant heat transfer, the temperature contours with $\theta = 0.35$ occur symmetrically near the side walls of the enclosure. The other temperature contours with $\theta \geq 0.4$ are nearly smooth curves which span from the middle-bottom of the enclosure and they are generally symmetric with respect to the vertical center line. With increase of the aspect ratio of the enclosure, the buoyant convection flow is increasingly strengthened, exhibiting a transformation from two square size recirculation rolls into a structure characterized by two rectangular high strength vortices. At $A = 1.0$, the circulation on each half of the cavity becomes stronger as they expand vertically and consequently, the temperature contour with $\theta = 0.15$ starts getting shifted towards the side wall and they break into two symmetric contour lines. The presence of significant convection is also exhibited in other temperature contour lines which start getting deformed and pushed towards the top plate.

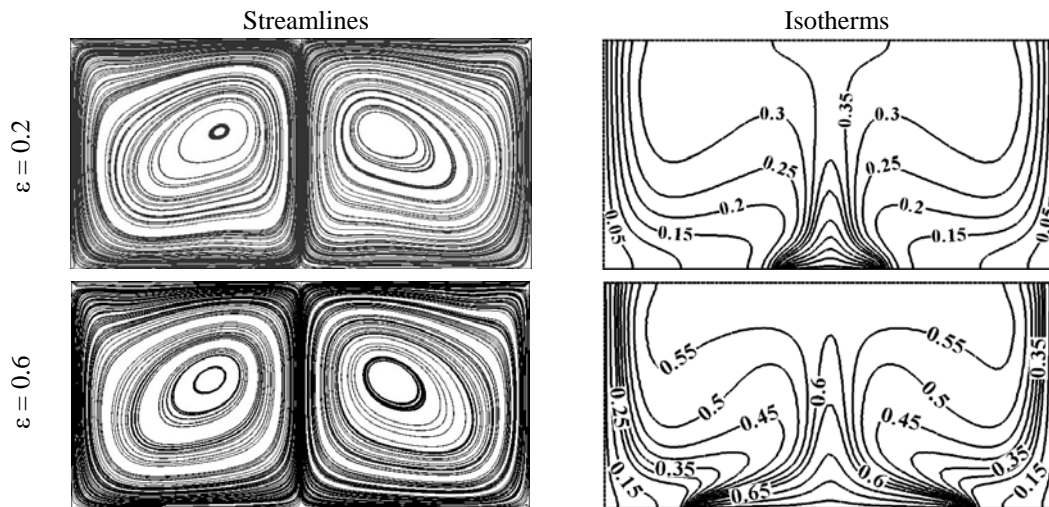


Fig. 4: Streamlines and isotherms for different heat source ratios ε with $A = 0.5$, $Gr = 10^6$, and $\Phi = 0^\circ$.

5.3 Effect of Discrete Heat Source Length:

The flow and temperature fields in terms of computed streamlines and isotherms for two representative values of the dimensionless source length $\varepsilon = 0.2$ and 0.6 are shown in Fig. 4. In each case, the flow descends downwards along the moving sidewalls and turns horizontally to the central region hitting the bottom wall. The circulation in each half of the cavity follows a progressive wrapping around the centers of rotation, and a more pronounced compression of the isotherms toward the boundary surfaces of the enclosure occur. Visual examination of the streamlines does not reveal any significant difference among the different cases. However, noticeable difference is observed in the isotherm plots. For $Gr = 10^6$, the temperature gradients near bottom and side walls tend to be significant leading to the development of a thermal boundary layer. Due to greater circulations near the central core at the top half of the enclosure, there are small gradients in temperature whereas a large stratification zone of temperature is observed at the vertical symmetry line due to stagnation of flow.

The convection region adjacent to the heat source becomes thinner and denser producing higher temperature gradients with increasing Gr . The heat transfer rate affect significantly with the increasing ε because the energy transport increases due to the increased area of the heated port. Since the isotherm plots change with Gr , it is the parameter of focus in the analysis for all cases. For $Gr \geq 10^4$, the buoyancy becomes dominant the heat transport and the isotherms with high values tend to concentrate near the heat source surface. It is noticed that the temperature decreases from the bottom to the top along the centerline of the cavity for a particular value of ε . At a fixed height, the temperature increases as the heat source length ε grows. The temperature profiles clearly express the heat transfer behavior expected from the isotherms given in Fig. 4, where the most intensive heat transfer region is located near the heat source surface due to the presence of large temperature gradients. The temperature gradients of the cooling air decrease as it ascends from the bottom. When the heat source length ε

increases, more heat is transferred into the system, thus the whole temperature level in the cavity is upgraded.

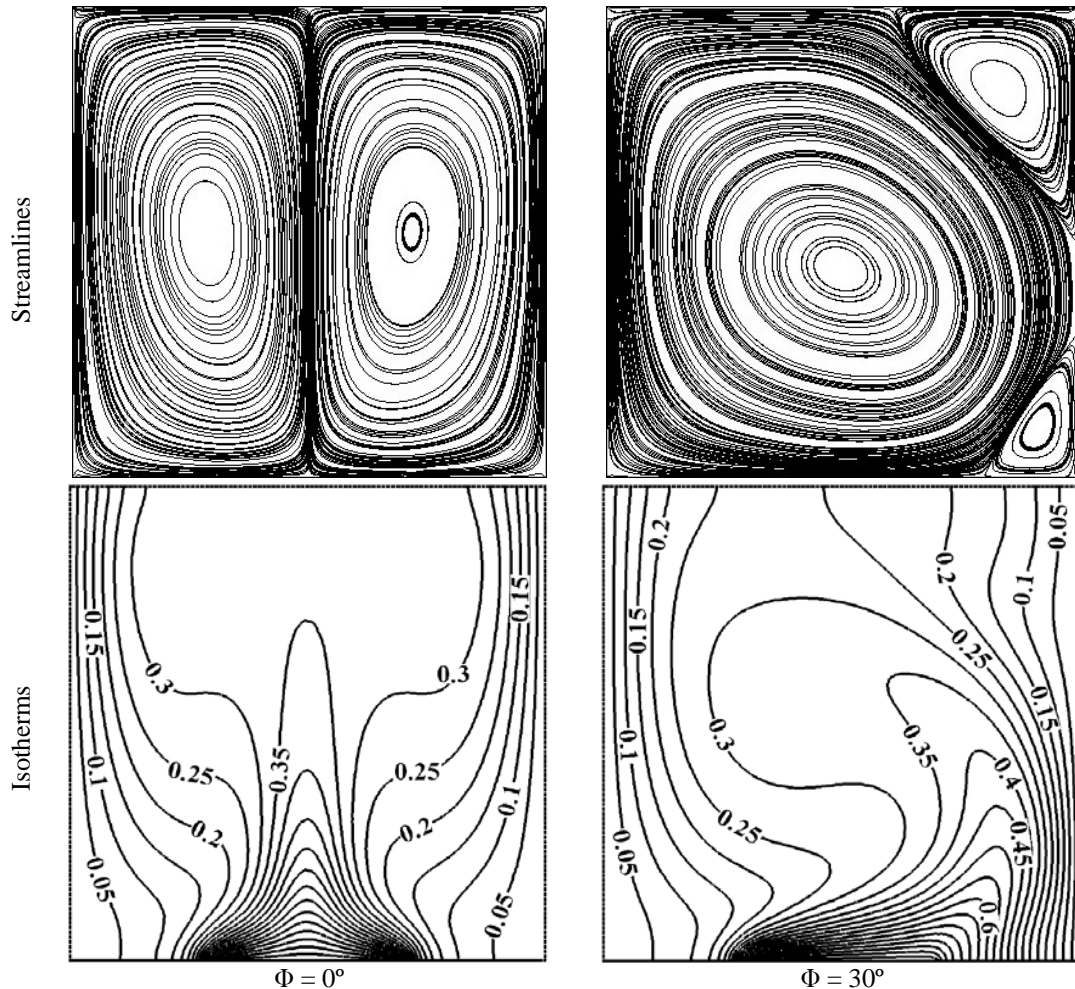


Fig. 5: Evolution of the flow in the enclosure with inclination angles for $A = 1$, $Gr = 10^5$, and $\epsilon = 0.4$.

5.4 Effect of Inclination Angles:

The evolution of the flow and thermal fields in the enclosure with increasing inclination are shown in Fig. 5 for a representative case of aspect ratio $A = 1$ and $Gr = 10^5$ with $\epsilon = 0.4$. It is observed that for horizontal cavity ($\Phi = 0^\circ$), where the buoyancy force is acting only in the y-direction, two recirculation cell is formed and the solution is symmetric about the vertical midline due to the symmetry of the problem geometry and boundary conditions. For the inclined enclosure this symmetry is completely destroyed due to the buoyancy force components acting in both x and y directions. The effect of cavity inclination is clearly visible on both the flow patterns and isotherms. This is evident at $\Phi = 30^\circ$, when the left recirculating vortex becomes dominating in the enclosure while the right vortex is squeezed thinner and ultimately is divided into two minor corner vortices. This circulation inside the cavity is greater near the center and least at the wall due to no slip boundary conditions. When Gr increases, the convection roll located at the left half of the square enclosure tends to merge in order to form a single large recirculation cell compared to two minor corner vortices. The isotherms are also adjusted according to the changes in the flow field and pushed towards the lower part of the right sidewall indicating the presence of a large temperature gradient there.

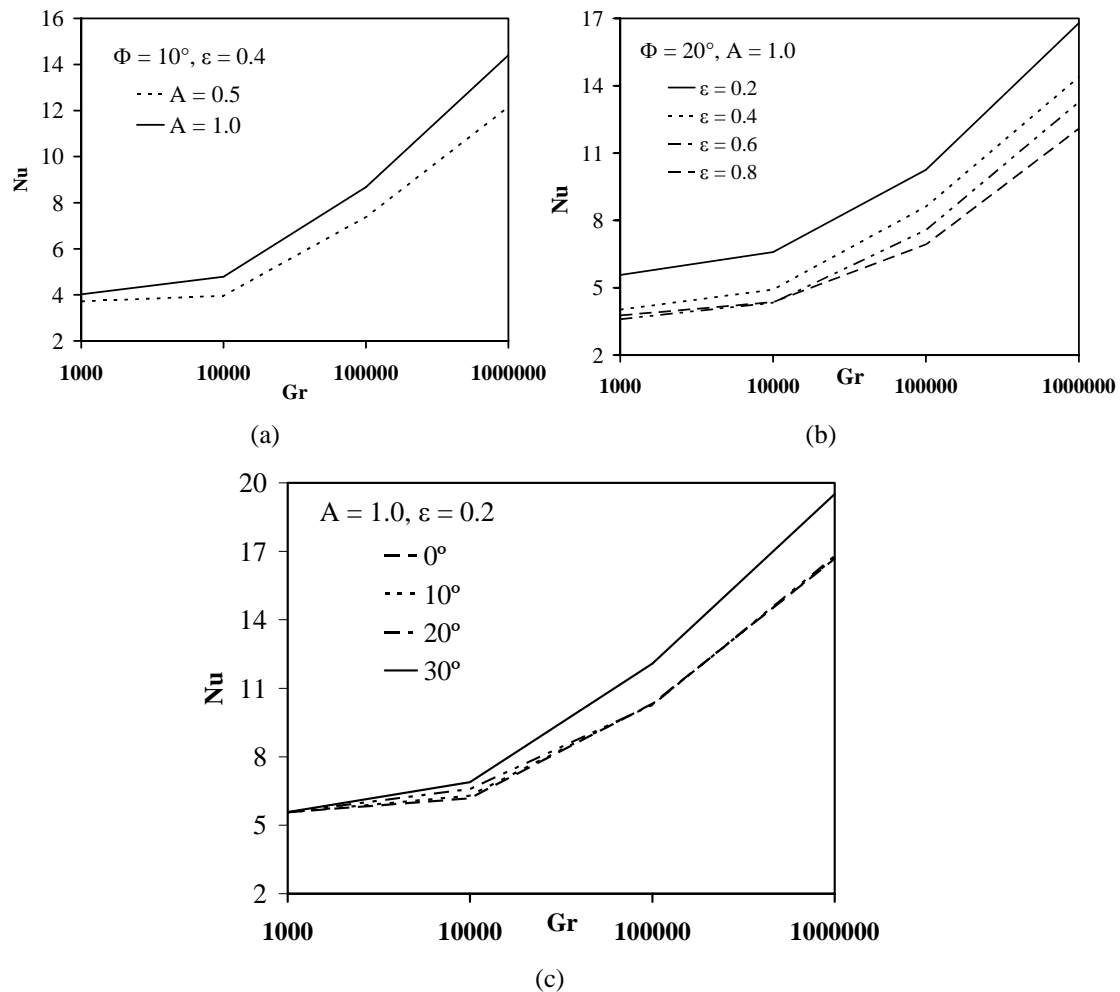


Fig. 6: Variation of the Nu at the heated surface with Gr for various (a) aspect ratios, (b) heat source sizes, (c) inclination angles.

5.5 Heat Transfer:

Next attention is focused upon the influence of the aspect ratio, inclination angle and discrete heat source size on the heat transfer rate across the discretely heated enclosure. The variation of the average Nusselt number, Nu, at the heated surface with Grashof number, Gr, for the entire set of the heated surface lengths (ϵ), aspect ratios (A), and cavity inclination angles (Φ) investigated are shown in Fig. 6(a), (b) and (c), respectively, from which some interesting trends are observed. In general, the average Nusselt number remains invariant up to a certain value of Grashof number and then increases briskly with increasing Grashof number. For low Grashof number, the curves maintain a flat trend that means low temperature gradients but Nu increases rapidly with Gr especially for $Gr > 10^4$. For a particular Grashof number, the average Nusselt number increases with increasing aspect ratio. These variations of the average Nusselt number differ greatly at higher Grashof number and vice versa. From these observations, it can be concluded that the overall heat transfer process improves as the aspect ratio increases until the cavity becomes square.

The variation of the average Nusselt number against Gr is shown in Fig. 6(b) for various values of ϵ . Concentrating on each plot separately for a particular value of ϵ , a trend of Nu increasing with Gr, is observed. When $Gr \geq 10^4$, the buoyancy aids more and more in the heat transfer process which results in more rapid increase of Nu. An important information obtained from this analysis is the effect of heat

source length on the heat transfer rate. Due to the symmetrical boundary conditions, two symmetric convection cells are generated and their interface behaves like an insulator. The centre of the heat source surface becomes the stagnation point of the heat transfer area, and attains the maximum temperature and minimum heat transfer rate. An increase in ε increases the rate of formation of convection cells which in turns decreases the average Nusselt number from the central area of the cavity. Maximum Nu is obtained at small heat source size for higher value of Gr while $\Phi = 0^\circ$ for $A = 0.5$ and $\Phi = 30^\circ$ for $A = 1.0$.

6. Conclusion

Natural convection in two-dimensional rectangular enclosure where the top wall is considered adiabatic, two vertical walls are maintained at constant low temperature, and the bottom wall is maintained at high temperature has been analyzed numerically using the finite element method. The resulting processes are investigated to yield quantitative results regarding the cooling effects. The main parameters of interest are Grashof number, Gr, the dimensionless heat source length, ε , the inclination angle with horizontal axis, Φ , and the aspect ratio of the cavity, A .

The resulting flow consists of two counter-rotating vortices. As far as the temperature field is concerned, at low values of Grashof number, the temperature is found to be more evenly distributed within the enclosure, and a relatively large region of the enclosure is affected by the heat source. As Grashof number increases and natural convection dominates, the temperature variation is restricted over a gradually diminishing region around the heat source. It is also noticed that the heat-affected region becomes larger with the increasing heat source length.

The average or overall Nusselt number increases mildly with cavity inclination for $Gr = 10^4$ while it increases much more rapidly at $\Phi = 30^\circ$ for higher Grashof number. The effect of enclosure aspect ratio on the average Nusselt number of the discrete heaters tends to improve with the increase of the Grashof number.

References

- Aydin, O. and Yang, J. (2000): Natural Convection in Enclosures with Localized Heating from Below and Symmetrically Cooling from Sides, *Int. J. Numer. Methods Heat Fluid Flow*, Vol. 10, pp. 518-529.
- Anderson, R. and Lauriat, G. (1986): The Horizontal Natural Convection Boundary Layer Regime in a Closed Cavity, in: *Proceedings of the Eighth International Heat Transfer Conference*, Vol. 4, pp. 1453-1458.
- Chu, H. H. S., Churchill, S. W. and Patterson, C. V. S. (1976): The Effects of Heaters Size, Location, Aspect Ratio, and Boundary Condition on Two-dimensional, Laminar Natural Convection in Rectangular Enclosure, *ASME J. Heat Transfer*, Vol. 98, pp. 194-201.
- Carmona, R. and Keyhani, M. (1989): The Cavity Width Effect on Immersion Cooling of Discrete Flush-heaters on One Vertical Wall of an Enclosure Cooled from the Top, *ASME J. Electronic Packaging*, Vol. 111, pp. 268-276.
- Chadwick, M. L., Webb, B. W. and Heaton, H. S. (1991): Natural Convection from Two-dimensional Discrete Heat Sources in a Rectangular Enclosure, *Int. J. Heat Mass Transfer*, Vol. 34, pp. 1679-1693.
- Elsherbiny, S. M., Raithby, G. D. and Hollands, K. G. T. (1982): Heat Transfer by Natural Convection Across Vertical and Inclined Air Layers, *J. Heat Transfer*, Vol. 104, pp. 96-102.
- Ganzarolli, M. M. and Milanez, L. F. (1995): Natural Convection in Rectangular Enclosures Heated from Below and Symmetrically Cooled from the Sides, *Int. J. Heat Mass transfer*, Vol. 38, pp. 1063-1073.
- Hasnaoui, M., Bilgen, E. and Vasseur, P. (1992): Natural Convection Heat Transfer in Rectangular Cavities Heated from Below, *J. Thermophys. Heat Transfer*, Vol. 6, pp. 255-264.
- Hsu, T. H. and Chen, C. K. (1996): Natural Convection of Micropolar Fluids in a Rectangular Enclosure, *Int. J. Engrg. Sci.*, Vol. 34, pp. 407-415.

- Incropera, F. P. (1988): Convection Heat Transfer in Electronic Equipment Cooling, ASME J. Heat Transfer, Vol. 110, pp. 1097-1111.
- Jaluria, Y. (1985): Natural Convection Cooling of Electronic Equipment. In Natural convection: Fundamental and Applications (Edited by S. Kakac et al.), pp. 961-986.
- Keyhani, K., Prasad, V. and Cox, R. (1988): An Experimental Study of Natural Convection in a Vertical Cavity with Discrete Heat Sources, ASME J. Heat Transfer, Vol. 110, pp. 616-624.
- Keyhani, M., Prasad, V., Shen, R. and Wong, T. T. (1988): Free Convection Heat Transfer from Discrete Heat Sources in a Vertical Cavity. In Natural and Mixed Convection in Electronic Equipment Cooling, ASME HTD, Vol. 100, pp. 13-24.
- Nguyen, T. H. and Prudhomme, M. (2001): Bifurcation of Convection Flows in a Rectangular Cavity Subjected to Uniform Heat Fluxes, Int. Comm. Heat Mass Transfer, Vol. 28, pp. 23-30.
- November, M. and Nansteel, M. W. (1986): Natural Convection in Rectangular Enclosures Heated from Below and Cooled Along One Side, Int. J. Heat Mass Transfer, Vol. 30, pp. 2433-2440.
- Ostrach, S. (1988): Natural Convection in Enclosures, J. Heat Transfer, Vol. 110, pp. 1175-1190.
- Prasad, V., Keyhani, M. and Shen, R. (1990): Free Convection in a Discretely Heated Vertical Enclosure: Effects of Prandtl Number and Cavity Size, ASME J. Electronic Packaging, Vol. 112, pp. 63-74.
- Papanicolaou, E. and Gopalakrishna, S. (1995): Natural Convection in Shallow, Horizontal Air Layers Encountered in Electronic Cooling, J. Electronic Packaging, Vol. 117, pp. 307-316.
- Refai Ahmed, G. and Yovanovich, M. M. (1991): Influence of Discrete Heat Source Location on Natural Convection Heat Transfer in a Vertical Square Enclosure, ASME J. Electronic Packaging, Vol. 113, pp. 268-274.
- Selamet, E. E., Arpaci, V. S. and Borgnkke, C. (1992): Simulation of Laminar Buoyancy Driven Flows in an Enclosure, Numer. Heat Transfer, Vol. 22, pp. 401-420.
- Sundstrom, L. G. and Kimura, S. (1996): On Laminar Free Convection in Inclined Rectangular Enclosures, J. Fluid Mech, Vol. 313, pp. 343-366.
- Sharif, M. A. R. and Mohammad, T. R. (2005): Natural Convection in Cavities with Constant Flux Heating at the Bottom Wall and Isothermal Cooling from the Sidewalls, Int. J. of Thermal Sciences, Vol. 44, pp. 865-878.
- Valencia, A. and Frederick, R. L. (1989): Heat Transfer in Square Cavities with Partially Active Vertical Walls, Int. J. Heat Mass Transfer, Vol. 32, pp. 1567-1574.
- Zienkiewicz, O. C., Taylor, R. L. (2000): The finite element method, 5th edition. Oxford: Butterworth-Heinemann.